Construction of risk prediction model using m6A RNA methylation regulators in prostate cancer: comprehensive bioinformatic analysis and histological validation

Yongjun Quan
Beijing Tongren Hospital
Xiaodong Zhang
Beijing Chaoyang Hospital
Hao Ping (pinghaotrh@ccmu.edu.cn)
Beijing Tongren Hospital https://orcid.org/0000-0002-4436-5170

Research Article

Keywords: prostate cancer, N6-methyladenosine (m6A), The Cancer Genome Atlas (TCGA), recurrence-free survival, m6Acluster, geneCluster, m6Ascore

Posted Date: October 19th, 2021

DOI: https://doi.org/10.21203/rs.3.rs-979251/v1

Version of Record: A version of this preprint was published at Cancer Cell International on January 19th, 2022. See the published version at https://doi.org/10.1186/s12935-021-02438-1.

Abstract

Background Epigenetic reprogramming reportedly has a crucial role in prostate cancer (PCa) progression. RNA modification is a hot topic in epigenetics, and N6-methyladenosine (m6A) accounts for approximately 60% of RNA chemical modifications. The aim of this study was to construct risk prediction model using m6A RNA regulators in PCa. Materials and methods Analyses were based on levels of 25 m6A regulators in The Cancer Genome Atlas (TCGA). Differential expression gene (DEG) and survival analyses were performed according to TCGA-PRAD clinicopathologic and follow-up information. To detect the influence of m6A regulators and their DEGs, consensus clustering analysis was performed, and tumor mutational burden (TMB) estimation and tumor microenvironment (TME) cell infiltration were assessed. mRNA levels of representative genes were verified using clinical PCa data. Results Diverse expression patterns of m6A regulators between tumor and normal (TN) were detected regarding Gleason score (GS), pathological T stage (pT), TP53 mutation, and survival comparisons, with HNRNPA2B1 and IGFBP3 being intersecting genes. HNRNPA2B1 was upregulated in advanced stages (GS > 7, pT3, HR >1, and TP53 mutation), as verified using clinical PCa tissue. Three distinct m6A modification patterns were identified through consensus clustering analysis but no significant difference was found among these groups in recurrence -free survival (RFS) analysis. Six DEGs of m6A clusters were screened through univariate Cox regression analysis. MMAB and PAIAP2 were intersecting genes for the five clinical factors. MMAB, which was upregulated in PCa compared with TN, was verified using clinical PCa samples. Three distinct subgroups were established according to the 6 DEGs. Cluster A involved the most advanced stages and had the poorest RFS. The m6A score (m6Ascore) was calculated based on the 6 genes, and the low m6Ascore group showed poor RFS with a negative association with infiltration of 16 of 23 immune-related cells. Conclusion We screened DEGs of m6A clusters and identified 6 genes (BAIAP2, TEX264, MMAB, JAGN1, TIMM8AP1, and IMP3), with which constructed a high predictive model with prognostic value by dividing TCGA-PRAD into three distinct subgroups and performing m6A core analysis. This study helps in elucidating the integral effects of m6A signaling on PCa progression.

Introduction

Prostate cancer (PCa) is a leading malignant tumor among men [1]. PCa has primarily been treated with surgical prostatectomy or androgen deprivation therapy (ADT). However, it can become castration-resistant PCa (CRPC), and biochemical recurrence or metastasis may occur during traditional therapy, which is the main cause of cancer-specific death. Therefore, elucidating the molecular mechanism related to PCa progression is crucial in the discovery of diagnostic biomarkers and therapeutic targets.

Epigenetic reprogramming is reported to have a crucial role in the progression of PCa [2]. Recently, RNA modification is being regarded as a hot topic in epigenetics research, and nearly 172 different RNA modifications are present in MODOMICS [3]. Among them, N6-methyladenosine (m6A) is widespread throughout the transcriptome; indeed, m6A comprises approximately 60% of RNA chemical modifications and is present on 0.1% to 0.4% of total adenosine residues, including > 300 noncoding RNAs and 7600 mRNAs, in eukaryotes [4-6]. RNA m6A methylation regulates mRNA alternative splicing, stability, and

intracellular localization, constituting the major posttranscriptional modification [7]. The formation of m6A is regulated by three categories of proteins: readers (recognize m6A-modified sites, such as YTHDC1, YTHDC2, YTHDF1, YTHDF2, YTHDF3, HNRNPC, FMR1, LRPPRC, HNRNPA2B1, IGFBP1, IGFBP2, IGFBP3, RBMX, and ELAVL1), writers (methyltransferases, such as METTL3, METTL14, METTL16, WTAP, VIRMA, ZC3H13, RBM15, RBM15B, and CBLL1), and erasers (demethylases, such as FTO and ALKBH5).

m6A regulatory genes are reported to participate in various carcinogenic and tumor progression processes [8, 9]. METTL3 is reported to advance PCa progression and was found to be related to poor prognosis by MYC and LEF1 and by stabilizing integrin β1 mRNA [10-12]. However, one study suggested that low expression of METTL3 is related to androgen receptor antagonists via upregulation of NR5A2/LRH-1 [13]. This finding indicates the controversy and opposing functions of METTL3 in PCa. YTHDF2-induced AKT phosphorylation and MDB3B m6A modification may also promote PCa proliferation, migration, and invasion [14, 15]. FTO, an m6A demethylase, inhibits the invasion and migration of PCa cells by regulating total m6A levels [16]. Nevertheless, there are insufficient data on m6A regulators in PCa, and the role of m6A regulators remains controversial; in general, comprehensive transcriptome and genomic analysis is needed. This study fully analyzed m6A-related genes in PCa progression and prognosis.

Materials And Methods

Data acquisition

Transcriptome profiling and simple nucleotide variation data for prostate adenocarcinoma in The Cancer Genome Atlas (TCGA) were downloaded from the GDC Data Portal (https://portal.gdc.cancer.gov/). Copy number and clinical phenotype data were downloaded from University of California Santa Cruz Xena (https://xena. ucsc.edu/). Gene expression matrices were extracted and obtained through Practical Extraction and Report Language (Perl) (version 5.34.0) and R software (4.0.3) (Vienna, Austria). The R package “RCircos” was used to draw Circos plots.

Differential expression gene (DEG) analysis

mRNA levels were analyzed with TPM (transcripts per kilobase of exome per million mapped reads) data, which were transformed from the HTSeq-FPKM transcriptome profiling data of TCGA-PRAD. The R packages “limma” and “ggpurb” were then used to identify DEGs between normal and tumor groups and for further statistical analysis. The Wilcoxon test was performed to determine DEG levels, and adjusted $P < 0.05$ was identified as statistically significant. The R packages “clusterProfiler” and “enrichplot” were used to analyze Gene Ontology (GO) and Kyoto Encyclopedia of Genes and Genomes (KEGG) pathway enrichment.

Survival & correlation analyses

Survival data for “biochemical_recurrence”, “days_to_first_biochemical_recurrence”, and “days_to_last_follow_up.diagnoses” were obtained from clinical phenotype data. When “days_to_first_biochemical_recurrence” was indicated, we regarded these patients as having “recurrence status”, and the time notated was used as the “recurrence follow-up time”. Other cases were regarded as having “no recurrence”, and “days_to_last_follow_up.diagnoses” was used as “recurrence_follow_up_time”. The R packages “survival” and “survminer” were used for survival analysis. Survival curves were evaluated through Kaplan–Meier and log-rank tests. Correlation analysis was performed through Spearman correlation analysis, and a prognostic network map was drawn using the R packages “igraph”, “psych”, “reshape2”, and “RColorBrewer”. To build a PCa prognostic model using DEGs of m6A clusters, univariate Cox regression analysis was conducted, and $P < 0.05$ was used for later gene consensus clustering analysis.

Consensus clustering analysis & principal component analysis (PCA)

To determine whether m6A regulators are related to PCa prognosis, the cohort from TCGA was allocated into different groups based on the consensus level of m6A regulators. The process was performed using the R package “ConsensusClusterPlus” and resulted in cluster consensus and item-consensus results. The graphical output consisted of heatmaps, consensus cumulative distribution function (CDF) plots and delta area plots. The cluster number was determined through a high consistency of clusters, a low coefficient of variation, and no significant increase in the CDF curve. The chi-square test or Fisher’s exact test was used to analyze clinicopathological characteristics and clustering. The heatmap was drawn through the R package “pheatmap”. Recurrence-free survival (RFS) was detected among groups using Kaplan–Meier and log-rank tests. PCA was performed to judge the fitness of the classification with the prcomp function of R software.

Tumor mutational burden (TMB) estimation

TMB was calculated by the total number of mutated/total covered bases [17]. PCa was classified into two groups based on the mean TMB status population. We analyzed the relationship between the m6A score (shown as m6Ascore below) and the TMB and then performed survival analysis comparing prognosis between high TMB and low TMB groups.

Tumor microenvironment (TME) cell infiltration

TME infiltration levels were calculated through single-sample gene set enrichment analysis (ssGSEA) and quantified using enrichment scores [18]. The gene set of each TME infiltrating immune cell type was obtained as previously reported [19]. Correlation analysis between m6Acluster or m6Ascore and immune-associated genes was performed to illustrate the relationship.

Clinical PCa samples

Forty-five pathologically diagnosed PCa patients (15 with Gleason score (GS) < 7, 15 with GS = 7, and 15 with GS > 7) were recruited from Beijing Tongren Hospital and Beijing Chaoyang Hospital in accordance with the Ethics Committee of Beijing Tongren Hospital and Beijing Chaoyang Hospital, affiliated with Capital Medical University. All patients underwent prostatectomy between 2016 and 2021; PCa and adjacent normal tissues were removed and stored in liquid nitrogen.

Quantitative real-time PCR (qPCR) analysis

qPCR analysis was performed as previously described by us [20, 21]. Total RNA was isolated using TRIzol™ reagent (Invitrogen) and Complementary DNA (cDNA) was synthesized through One-Step gDNA Removal and cDNA Synthesis SuperMix (TransGen Biotech, Beijing, China). qPCR was performed using Top Green qPCR SuperMix (TransGen Biotech) on an SDS 7500 FAST Real-Time PCR system (Applied Biosystems, Foster City, CA, USA). GAPDH or 18S ribosomal RNA was used as endogenous reference gene. The relevant primer sequences are shown in Supplementary Table 1.

Statistical analysis

Statistical analyses were conducted using R software (4.0.3) and GraphPad Prism 7.0 (GraphPad Software, La Jolla, CA, USA). Incomplete data were excluded. Chi-square or Fisher's exact tests were used for categorical variables and Wilcoxon or Kruskal-Wallis tests for continuous data. Correlations between two levels were assessed through Pearson and Spearman correlation analysis. Survival analysis was applied through the log-rank test of Kaplan-Meier survival analysis and hazard ratio (HR) with the 95% confidence interval (CI) of univariate Cox proportional hazard models. $P < 0.05$ was indicated as significant.

Results

Characteristics of m6A regulators in PCa

In the dataset TCGA-PRAD, we analyzed CNV alterations, DEGs, and the mutation frequency of m6A regulators of PCa through comparison with normal samples. For CNV events, approximately 72% (18/25) of m6A regulators lost DNA copy number, with ZC3H14 having the highest degree of copy number loss (28.49%) (Fig. 1A). Six m6A regulators gained copy number, among which VIRMA had the highest percentage (3.19%) (Fig. 1Aa). The m6A regulator CNV alterations and locations on chromosomes are shown in Fig. 1Ab. Of the 499 tumor and 52 normal samples in the dataset from TCGA, DEGs of m6A regulators were statistically estimated using TPM data. Levels of METTL3, HNRNPA2B1, RBM15B, and IGFBP2 were higher and ZC3H13, FTO, and IGFBP3 lower in PCa tissues than in normal tissues ($P < 0.001$) (Fig. 1B). In mutation frequency analyses, 17 samples (3.51%) showed mutations in m6A-related

genes; mutation of YTHDC2, RBM15B, YTHDF2, and IGFBP1 was detected in one sample (Fig. 1D). All 25 m6A regulators exhibited low mutation rates (< 1%) in TCGA samples.

Expression of m6A regulators in PCa prognosis and different clinicopathological characteristics

Expression of m6A regulators in different GSs and pathological T (pT) stages was estimated using TCGA-PARD TPM data. As PCa with GS ≥ 7 is associated with worse prognosis [22, 23], the PCa samples were divided into three groups: GS < 7, GS = 7, and GS > 7. Compared with the GS < 7 group, IGFBP3, HNRNPA2B, RBMX, RBM15B, YTHDF1, HNRNPC, and VIRMA were significantly highly expressed in the GS > 7 group (P < 0.001) (Fig. 2A). In addition, T2 (188), T3 (295), and T4 (10) of pT stages were compared. Among the 25 m6A regulators, IGFBP3, HNRNPA2B1, VIRMA, and RBMX were more highly expressed in T3 stage than in T2 stage (P < 0.001) (Fig. 2A). Based on Kaplan-Meier curves in survival analysis, high expression of HNRNPA2B1, IGFBP1, and ELAVL1 was associated with poor RFS (P < 0.001) (Fig. 1C). Moreover, TP53 mutation in PCa was associated with shorter radiographic progression-free survival (rPFS) and time to CRPC [24]. Compared with the TP53 wild-type group of PCa samples, levels of VIRMA and IGFBP3 were higher and IGFBP2 lower in the TP53 mutation group (Fig. 2D). Risk factors and relationships of m6A regulators are summarized in the prognosis network shown in Fig. 2E.

We analyzed DEGs of m6A regulators in GS (GS > 7 versus (vs.) GS < 7), pT (T3 vs. T2), RFS (P value of univariate Cox regression analysis < 0.05), TN (tumor vs. normal PCa tissues), and TP53 (mutation vs. wild type) comparisons. Intersecting genes were identified via a Venn diagram, and HNRNPA2B1 and IGFBP3 were differentially expressed in all comparisons (Fig. 2F). The level of HNRNPA2B1 was higher in the PCa group than in the normal group and also high in association with advanced-stage parameters, namely, GS > 7, pT3, HR >1, and TP53 mutation. However, the level of IGFBP3 was lower in PCa tissues but higher in the presence of the above advanced-stage indicators. This suggests that different molecular mechanisms and expression patterns may exist in PCa and progression. We then assessed expression of HNRNPA2B1 and IGFBP3 in 45 PCa tissues and 15 adjacent normal prostate tissues. Levels of HNRNPA2B1 and IGFBP3 were higher in 66.7% (10/15, P < 0.05) and 40.0% (6/15, P > 0.05) of PCa tissues than in adjacent normal tissues, respectively, and the GS > 7 group exhibited elevated expression of HNRNPA2B1 and IGFBP3 compared with the GS < 6 group (both P < 0.05) (Fig. 2G).

Consensus clustering analysis according to m6A regulators

To further explore the phenotypes of m6A regulators in different prognoses and clinicopathological characteristics of the cohort TCGA-PRAD, we performed consensus clustering analysis to identify subgroups of 495 PARD cases according to 25 m6A regulators (m6Acluster). Relatively high consistency, a low coefficient of variation, and an appreciable increase in the area under the CDF curve were determined as the criteria of cluster number. With regard to the relative change in the area under the CDF curves for the cluster number, k = 3 was determined to be the best category number of clusters (Fig. 3A).

Subclasses were evaluated via PCA, and all 3 clusters were significantly distinguished (Fig. 3B), indicating correct prediction of the m6Acluster (these clusters are shown as “clusters 1–3 or A-C”). Next, we compared different clinicopathological characteristics of PRAD between the clusters, and the results showed relatively higher pathological N (pN) stage, GS 8–10, and biochemical recurrence rates in cluster A (Fig. 3C). The different KEGG pathways between clusters A and C are depicted in Fig. 3D. We also analyzed changes in immune cell infiltration in different m6A clusters and found 12 of 23 subpopulations of immune cells to be differentially expressed in the three clusters (Fig. 3E). Kaplan-Meier survival curves of RFS based on the m6Aclusters demonstrated no significant differences among the groups (P = 0.475) (Fig. 3F).

Consensus clustering analysis based on DEGs of m6A clusters

DEGs (P value of Bayes test < 0.001) were analyzed in every pairwise comparison according to the three clusters based on m6A regulators, and the 74 intersecting genes were identified via a Venn diagram (Fig. 4A). We then analyzed the biological functions of these 74 genes, which were categorized into GO terms of biological process (BP), cell component (CC), and molecular function (MF). Under the stringent threshold of P-adjust < 0.05, only 1 specific CC (proton-transporting V-type ATPase, V0 domain) was enriched (Fig. S1A-B). Additionally, KEGG signaling pathway analysis of 74 genes indicated significant enrichment in the oxidative phosphorylation KEGG pathway (Fig. S1C-D).

Univariate Cox regression analysis was also performed on the 74 intersecting genes, and 6 (BAIAP2, TEX264, MMAB, JAGN1, TIMM8AP1, and IMP3) related to PCa recurrence were selected (P < 0.05) (Fig. 4B). The characteristics of the 6 genes regarding CNV alterations, DEGs, and mutation frequency were analyzed in PCa compared with normal samples (Fig. S2A-D). We found that levels of 4 of the 6 genes were significantly upregulated in PCa tissues. When assessing expression of the 6 genes with respect to the clinicopathological characteristics GS, pT, and TP53, we found that most were downregulated in advanced stages (GS > 7, pT3, and TP53 mutation). Survival analysis also indicated that high expression of these 6 genes was significantly associated with poor RFS (Fig. S3A-D). The risk factors and relationships of the 6 genes are summarized in the prognosis network illustrated in Fig. S3E.

Consensus clustering analysis was performed for these 6 genes (geneCluster), and k = 3 was determined to be the best classification in the delta area results (cluster 1–3 or A-C) (Fig. 4C). PCA verified the significance of the three subgroups (Fig. S4A).

A heatmap of clinicopathological features in the three geneClusters indicated that pT stage, N stage, GS, and biological recurrence were significantly higher in geneCluster A than in the other clusters (Fig. 4D). Among the m6Aclusters, Kaplan-Meier survival analysis revealed significant differences between the three clusters, among which geneCluster A had the poorest RFS (P = 0.012) (Fig. 3E). Next, we analyzed expression of m6A regulators in different geneClusters and found that 21 of 25 m6A regulators were differentially expressed among them (Fig. 4F). Moreover, 16 of 23 subpopulations of immune cells were

differentially expressed among the three clusters (Fig. S4B). The different KEGG pathways between the A and C geneClusters are shown in Fig. S4C.

We also analyzed DEGs of the 6 genes regarding GS, pT, RFS, TN, and TP53, as illustrated in Fig. 2G. The intersecting genes MMAB and BAIAP2 were identified via a Venn diagram (Fig. 4G), and both were highly expressed in PCa tissues compared with normal tissue but low in the four parameters indicating advanced stage. This suggests opposite expression patterns of MMAB and PAIAP2 in PCa occurrence and progression. Expression of MMAB was analyzed and found to be upregulated in 60.0% (9/15, $P < 0.05$) of PCa tissues compared with adjacent normal tissues, with the GS > 7 group exhibiting reduced expression compared with the G < 7 group ($P < 0.05$) (Fig. 4H).

Low m6Ascore based on the 6 genes was associated with poor prognosis in RFS

The m6Ascore was calculated through PCA of the 6 gene levels in TCGA-PARD, and the Kruskal-Wallis test was performed to examine the relationship between m6Ascore and geneCluster/m6Acluster. The results revealed a significant difference in both clusters: geneCluster A had the lowest m6Ascore and geneCluster C the highest (Fig. 5A). PRAD patients were divided into two groups based on the optimum threshold segmentation of m6Ascore in RFS analysis, and according to Kaplan-Meier survival analysis, poor RFS was associated with the low m6Ascore group (Fig. 5B). The alluvial diagram shows the changes in m6Acluster, geneCluster, m6Ascore, and recurrence status (fustat) (Fig. 5C). The correlation of m6Ascore and immune-associated genes was evaluated, resulting in 16 of 23 immune-related cell infiltrates being negatively related to m6Ascore (Fig. 5D).

Characteristics of m6Ascore status for TCGA-PRAD tumor mutation and subtypes

As shown in Fig. 5B, TCGA-RRAD patients were divided into two groups (58 in the low m6Ascore group and 437 in the high m6Ascore group), and the association of m6Ascore and TMB was assessed. The results showed significant association between either and TMB ($P > 0.05$) (Fig. 6A). The PRAD patients were also divided into two groups based on TMB according to the same method (242 in the low TMB group and 231 in the high TMB group). In Kaplan-Meier analysis, a tendency toward poor RFS was found in the high TMB group compared with the low TMB group, but with no significance ($P = 0.051$). When analyzing m6A and TMB together, we found that a great RFS advantage for the combination of low TMB with high m6Ascore (Fig. 6B). The distribution differences of somatic mutations were analyzed between m6Ascore groups, and the results indicated a more extensive association between TMB and TP53 (18% vs. 8%) but a reduce one for SPOP (2% vs. 12%) in the low m6Ascore group (Fig. 6C). For the relationship between m6Ascore and fustat, the low m6Ascore group experienced a higher rate of recurrence, which was also associated with a lower m6Ascore (Fig. 6D). We then analyzed prognosis in the m6Ascore groups with regard to different clinicopathological features through RFS analysis (Fig. 6E and Fig. S5A-

B), and the low m6Ascore group was related to poor RFS and GS 8–10 and pT3 stage ($P < 0.05$) (Fig. 6E). To detect potential response to immunotherapy, expression of PD-L1 was detected, and the low m6Ascore group showed relatively high levels of expression (Fig. 6F). Finally, we performed IPS analysis to examine anti-PD1 and/or anti-CTLA4 treatment and found no significant difference between the low and high m6Ascore groups (Fig. 6G, Fig. S5C).

Discussion

In this study, we comprehensively analyzed m6A regulators in TCGA-PRAD and found 6 DEGs (BAIAP2, TEX264, MMAB, JAGN1, TIMM8AP1, and IMP3) based on m6Aclusters. First, we established a model of optimal clusters and performed m6Ascore analysis based on the above 6 genes.

In general, elucidating the molecular mechanism of PCa progression remain crucial. It has been reported that epigenetic reprogramming is key for PCa progression [25, 26] and that inhibition of the epigenetic regulator EZH2 might effectively overcome ADT resistance [2]. Our previous study found that epigenetically activating AR/NDRG1 signaling through histone methylation and DNA methylation significantly suppresses CRPC progression [20, 21].

Nevertheless, the effect of posttranscriptionally regulating RNA modification in PCa is still unclear. m6A RNA methylation may be among the most extensive RNA modifications [27-29]. Yabing Chen et al highlighted that total RNA m6A modification levels are significantly increased in PCa tissues due to upregulation of METTL3 [30]. In addition, knockdown of METTL3 significantly reduces PCa cell migration and invasion. YTHDF2, a reader of m6A modification, synergistically induces PCa progression with METTL3 by regulating AKT phosphorylation [31]. However, low levels of METTL3 were also found to lead to advanced metastatic PCa that is resistant to androgen receptor antagonists [32]. These controversial results reveal the uncertain roles of individual m6A regulators in PCa, and various m6A regulators may form a complex network structure and interact with each other to affect PCa progression.

In this study, we examined three representative groups of m6A regulators: 14 “readers”, 9 “writers”, and 2 “erasers”. Bioinformatic analysis was then performed to comprehensively investigate the association between m6A regulators and PCa clinicopathological characteristics and prognosis.

In survival and Cox regression analyses, we evaluated RFS instead of overall survival (OS) because only 10 of 493 TCGA-PARD patients died, making it difficult to obtain statistically significant results by assessing OS. In our RFS analysis, “biochemical_recurrence” and “days_to_first_biochemical_recurrence” data did not coincide, and we finally used the “days_to_first_biochemical_recurrence” data to confirm “recurrence status” and “recurrence follow-up time”.

The landscape of m6A variation in PCa was recently reported [33-38], though none have analyzed sufficient m6A regulators and verified them using clinical PCa tissues. To overcome these shortcomings, we explored all 25 widely acknowledged m6A regulators and assessed associations of various clinicopathological characteristics, such as TN, GS, pT, TP53 mutation, and survival analysis of RFS,

using TCGA-PRAD data. Additionally, we analyzed DEGs of m6A regulators in relation to the five factors, and the intersecting genes (HNRNPA2B1 and IGFBP3) were verified with clinical PCa tissues. The level of HNRNPA2B1 was higher in PCa tissues than in normal prostate tissues and high in correlation with the other four advanced factors. However, the level of IGFBP3 was lower in PCa tissues but higher in the presence of the above advanced-stage indicators. This suggests that independent molecular mechanisms and expression patterns exist in PCa and its progression. Consistent with bioinformatic analysis, mRNA levels of HNRNPA2B1 and IGFBP3 were elevated in PCa tissue of the high GS group (GS > 7) compared with the low GS group (GS < 7). In TN comparison, expression of HNRNPA2B1 was higher in PCa, but no significant difference in the level of IGFBP3 expression was found.

It has been reported that upregulation of HNRNPA2B1 by PCAT6 promotes PCa progression and neuroendocrine differentiation [39]. HNRNPA2B1 may also be an independent prognostic factor and contribute to cancer progression [40]. Coexpression network analysis using clinical data from the GSE70768 dataset as well as quantitative proteomic mass spectrometry profiling and gene enrichment analysis using LNCaP and PC3 cell lines suggest that HNRNPA2B1 is associated with PCa progression and prognosis [41, 42]. The level of IGFBP3 in PCa is controversial, with one meta-analysis indicating that the CC genotype of the IGFBP3–202A/C polymorphism is associated with an increased risk of PCa [43-45]. Overall, tissue verification and previous studies support a certain level of accuracy of our bioinformatic analysis using TCGA-PRAD data.

To analyze the overall effects of m6A regulators in PCa, we performed consensus clustering analysis and divided the cohort TCGA-PRAD into 3 subgroups based on 25 m6A regulators. As no significant difference in the 3 clusters for RFS was observed, this cluster analysis with m6A regulators may not be suitable for inclusion in a prognostic risk prediction model.

As epigenetic regulators, posttranscriptional modification of target genes is the primary function of m6A regulators. To analyze the downstream genes of m6A regulators, we focused on the DEGs of m6A cluster and screened six risk genes (BAIAP2, TEX264, MMAB, JAGN1, TIMM8AP1, and IMP3) through univariate Cox regression analysis. Only IMP3 has previously been reported in PCa studies, and it appears to be increased in PCa tissues and associated with higher GS, PCa metastasis, and PCa-specific survival [46-48]. Regardless, according to our bioinformatic analysis of TCGA-PRAD, expression of IMP3 was decreased in three groups related to advanced PCa (HR (RFS) < 1, TP53 mutation < wild type, pT3 < pT2, and tumor > normal). This finding indicates discordance between TCGA-PRAD data and previous result, warranting further confirmation.

Consensus clustering analysis was then performed based on the six genes to construct a risk prediction model, and TCGA-PARD patients were divided into 3 subgroups. In these clusters, the clinicopathological parameters PSA grade 3 (grade 1: 0 > and < 1, grade 2: 1–10, grade 3: > 10), pT 4, pN 1, and GS > 7 grouped in cluster A in relation to significantly poor RFS, suggesting an accurate risk prediction model based on 6 genes. We then analyzed the DEGs of the 6 genes in correlation with the above five factors, and MMAB and BAIAP2 were identified as intersecting genes. Levels of both were higher in PCa tissues

than in adjacent normal prostate tissues but lower in tissues with advanced-disease factors. We next verified MMAB based on different GSs of PCa tissues and adjacent normal tissues and found its level of mRNA to be elevated in PCa tissues but decreased in the GS > 8 group, consistent with the bioinformatic analysis.

To quantitatively illustrate the m6A signature, we calculated m6Ascore according to the expression of the 6 genes in TCGA-PARD: m6Ascore correlated positively with geneCluster, and lower m6Ascore was related to poor prognosis. Furthermore, m6Ascore was negatively related to 16 of 23 immune-associated cells. Thus, a potential mechanism by which the m6A signature protects against PCa progression is by negatively regulating immune cell infiltration. A high TMB score is related to tumor-related mutations and sensitivity to immunotherapy [49, 50], and Yue Zhao et al reported that m6A modification in PCa may contribute to immunotherapy strategies [33]. In our study, the lower m6Ascore group tended to have a higher proportion of TP53 mutations (18%), and the high m6Ascore group tended to have a higher proportion of SPOP mutations. However, no significant correlation with TMB was found in our study, and there were also no differences in PD-L1 expression or IPS score with anti-PD1 and/or anti-CTLA4 treatment. In summary, results of this study do not clearly support an influence of m6A modification on PCa immune cell infiltration and immunotherapy.

Conclusions

In this study, we comprehensively analyzed m6A regulators in TCGA-PRAD through bioinformatic analysis and tissue validation. First, we screened DEGs of m6Aclusters and found 6 genes (BAIAP2, TEX264, MMAB, JAGN1, TIMM8AP1, and IMP3), through which we divided PCa patients into 3 subgroups and calculated m6Ascore to construct a risk model with high predictive value for recurrence. This study may contribute to illustrating the effects of m6A signaling on the progression and prognosis of PCa.

Abbreviations

PCa: prostate cancer; ADT: androgen deprivation therapy; CRPC: castration-resistant prostate cancer; m6A: N6-methyladenosine; TCGA: The Cancer Genome Atlas; DEG: differentially expressed gene; GO: Gene Ontology; KEGG: Kyoto Encyclopedia of Genes and Genomes; PCA: principal component analysis; CDF: cumulative distribution function; RFS: recurrence-free survival; TMB: tumor mutational burden; ssGSEA: single-sample gene set enrichment analysis; GS: Gleason score; HR: hazard ratio; CI: confidence interval; pT: pathological T; pN: pathological N; rPFS: radiographic progression-free survival; pN: pathological N; OS: overall survival.

Declarations

Acknowledgments

We thank Beijing Chaoyang Hospital, Capital Medical University for providing samples from PCa patients.

Author contributions

Yongjun Quan designed the study and performed the qPCR analysis. Hao Ping analyzed the data. Xiaodong Zhang and Hao Ping provided the clinical prostate cancer samples. Yongjun Quan wrote the manuscript, which was approved by all authors.

Funding

This study was supported by the National Natural Science Foundation of China (Grant No. 81772698 and 82072833 to Hao Ping) and Open Research Fund from Beijing Advanced Innovation Center for Big Data-Based Precision Medicine, Beijing Tongren Hospital, Beihang University & Capital Medical University (Grant No. BHTR-KFJJ-202005 to Hao Ping).

Availability of data and materials

The data and materials supporting the conclusions of this study are included within the article and its additional files.

Ethics approval and consent to participate

Human prostate samples were provided by Beijing Tongren Hospital and Beijing Chaoyang Hospital. Ethical consent was approved by the Ethics Committee of Beijing Tongren Hospital and Beijing Chaoyang Hospital, affiliated with Capital Medical University.

Consent for publication

All authors read and approved the final manuscript for publication.

Competing interests

The authors declare that they have no competing interests.

References

[1] Siegel RL, Miller KD and Jemal A. Cancer statistics, 2019. CA Cancer J Clin 2019; 69: 7-34.

[2] Xiao L, Tien JC, Vo J, Tan M, Parolia A, Zhang Y, Wang L, Qiao Y, Shukla S, Wang X, Zheng H, Su F, Jing X, Luo E, Delekta A, Juckette KM, Xu A, Cao X, Alva AS, Kim Y, MacLeod AR and Chinnaiyan AM.

Epigenetic Reprogramming with Antisense Oligonucleotides Enhances the Effectiveness of Androgen Receptor Inhibition in Castration-Resistant Prostate Cancer. Cancer Res 2018; 78: 5731-5740.

[3] Boccaletto P, Machnicka MA, Purta E, Piatkowski P, Baginski B, Wirecki TK, de Crécy-Lagard V, Ross R, Limbach PA, Kotter A, Helm M and Bujnicki JM. MODOMICS: a database of RNA modification pathways. 2017 update. Nucleic Acids Res 2018; 46: D303-d307.

[4] Cantara WA, Crain PF, Rozenski J, McCloskey JA, Harris KA, Zhang X, Vendeix FA, Fabris D and Agris PF. The RNA Modification Database, RNAMDB: 2011 update. Nucleic Acids Res 2011; 39: D195-201.

[5] Meyer KD, Saletore Y, Zumbo P, Elemento O, Mason CE and Jaffrey SR. Comprehensive analysis of mRNA methylation reveals enrichment in 3' UTRs and near stop codons. Cell 2012; 149: 1635-1646.

[6] Dubin DT and Taylor RH. The methylation state of poly A-containing messenger RNA from cultured hamster cells. Nucleic Acids Res 1975; 2: 1653-1668.

[7] Maity A and Das B. N6-methyladenosine modification in mRNA: machinery, function and implications for health and diseases. Febs j 2016; 283: 1607-1630.

[8] Tuncel G and Kalkan R. Importance of m N(6)-methyladenosine (m(6)A) RNA modification in cancer. Med Oncol 2019; 36: 36.

[9] Lin S, Choe J, Du P, Triboulet R and Gregory RI. The m(6)A Methyltransferase METTL3 Promotes Translation in Human Cancer Cells. Mol Cell 2016; 62: 335-345.

[10] Ma XX, Cao ZG and Zhao SL. m6A methyltransferase METTL3 promotes the progression of prostate cancer via m6A-modified LEF1. Eur Rev Med Pharmacol Sci 2020; 24: 3565-3571.

[11] Yuan Y, Du Y, Wang L and Liu X. The M6A methyltransferase METTL3 promotes the development and progression of prostate carcinoma via mediating MYC methylation. J Cancer 2020; 11: 3588-3595.

[12] Li E, Wei B, Wang X and Kang R. METTL3 enhances cell adhesion through stabilizing integrin β1 mRNA via an m6A-HuR-dependent mechanism in prostatic carcinoma. Am J Cancer Res 2020; 10: 1012-1025.

[13] Cotter KA, Gallon J, Uebersax N, Rubin P, Meyer KD, Piscuoglio S, Jaffrey SR and Rubin MA. Mapping of m6A and Its Regulatory Targets in Prostate Cancer Reveals a METTL3-low Induction of Therapy Resistance. Mol Cancer Res 2021;

[14] Du C, Lv C, Feng Y and Yu S. Activation of the KDM5A/miRNA-495/YTHDF2/m6A-MOB3B axis facilitates prostate cancer progression. J Exp Clin Cancer Res 2020; 39: 223.

[15] Li J, Xie H, Ying Y, Chen H, Yan H, He L, Xu M, Xu X, Liang Z, Liu B, Wang X, Zheng X and Xie L. YTHDF2 mediates the mRNA degradation of the tumor suppressors to induce AKT phosphorylation in N6-

methyladenosine-dependent way in prostate cancer. Mol Cancer 2020; 19: 152.

[16] Zhu K, Li Y and Xu Y. The FTO m(6)A demethylase inhibits the invasion and migration of prostate cancer cells by regulating total m(6)A levels. Life Sci 2021; 271: 119180.

[17] Chen DS and Mellman I. Elements of cancer immunity and the cancer-immune set point. Nature 2017; 541: 321-330.

[18] Hänzelmann S, Castelo R and Guinney J. GSVA: gene set variation analysis for microarray and RNA-seq data. BMC Bioinformatics 2013; 14: 7.

[19] Zhang B, Wu Q, Li B, Wang D, Wang L and Zhou YL. m(6)A regulator-mediated methylation modification patterns and tumor microenvironment infiltration characterization in gastric cancer. Mol Cancer 2020; 19: 53.

[20] Quan Y, Cui Y, Wahafu W, Liu Y, Ping H and Zhang X. MLL5α activates AR/NDRG1 signaling to suppress prostate cancer progression. Am J Cancer Res 2020; 10: 1608-1629.

[21] Quan Y, Zhang X, Butler W, Du Z, Wang M, Liu Y and Ping H. The role of N-cadherin/c-Jun/NDRG1 axis in the progression of prostate cancer. International Journal of Biological Sciences 2021; 17: 3288-3304.

[22] Eggener SE, Scardino PT, Walsh PC, Han M, Partin AW, Trock BJ, Feng Z, Wood DP, Eastham JA, Yossepowitch O, Rabah DM, Kattan MW, Yu C, Klein EA and Stephenson AJ. Predicting 15-year prostate cancer specific mortality after radical prostatectomy. J Urol 2011; 185: 869-875.

[23] Kozminski MA, Tomlins S, Cole A, Singhal U, Lu L, Skolarus TA, Palapattu GS, Montgomery JS, Weizer AZ, Mehra R, Hollenbeck BK, Miller DC, He C, Feng FY and Morgan TM. Standardizing the definition of adverse pathology for lower risk men undergoing radical prostatectomy. Urol Oncol 2016; 34: 415 e411-416.

[24] Deek MP, Van der Eecken K, Phillips R, Parikh NR, Isaacsson Velho P, Lotan TL, Kishan AU, Maurer T, Boutros PC, Hovens C, Abramowtiz M, Pollack A, Desai N, Stish B, Feng FY, Eisenberger M, Carducci M, Pienta KJ, Markowski M, Paller CJ, Antonarakis ES, Berlin A, Ost P and Tran PT. The Mutational Landscape of Metastatic Castration-sensitive Prostate Cancer: The Spectrum Theory Revisited. Eur Urol 2021;

[25] Van Neste L, Groskopf J, Grizzle WE, Adams GW, DeGuenther MS, Kolettis PN, Bryant JE, Kearney GP, Kearney MC, Van Criekinge W and Gaston SM. Epigenetic risk score improves prostate cancer risk assessment. Prostate 2017; 77: 1259-1264.

[26] Natesan R, Aras S, Effron SS and Asangani IA. Epigenetic Regulation of Chromatin in Prostate Cancer. Adv Exp Med Biol 2019; 1210: 379-407.

[27] Desrosiers R, Friderici K and Rottman F. Identification of methylated nucleosides in messenger RNA from Novikoff hepatoma cells. Proc Natl Acad Sci U S A 1974; 71: 3971-3975.

[28] Alarcón CR, Lee H, Goodarzi H, Halberg N and Tavazoie SF. N6-methyladenosine marks primary microRNAs for processing. Nature 2015; 519: 482-485.

[29] Patil DP, Chen CK, Pickering BF, Chow A, Jackson C, Guttman M and Jaffrey SR. m(6)A RNA methylation promotes XIST-mediated transcriptional repression. Nature 2016; 537: 369-373.

[30] Chen Y, Pan C, Wang X, Xu D, Ma Y, Hu J, Chen P, Xiang Z, Rao Q and Han X. Silencing of METTL3 effectively hinders invasion and metastasis of prostate cancer cells. Theranostics 2021; 11: 7640-7657.

[31] Li J, Xie H, Ying Y, Chen H, Yan H, He L, Xu M, Xu X, Liang Z, Liu B, Wang X, Zheng X and Xie L. YTHDF2 mediates the mRNA degradation of the tumor suppressors to induce AKT phosphorylation in N6-methyladenosine-dependent way in prostate cancer. Molecular cancer 2020; 19: 152-152.

[32] Cotter KA, Gallon J, Uebersax N, Rubin P, Meyer KD, Piscuoglio S, Jaffrey SR and Rubin MA. Mapping of m(6)A and Its Regulatory Targets in Prostate Cancer Reveals a METTL3-Low Induction of Therapy Resistance. Mol Cancer Res 2021; 19: 1398-1411.

[33] Zhao Y, Sun H, Zheng J and Shao C. Analysis of RNA m(6)A methylation regulators and tumour immune cell infiltration characterization in prostate cancer. Artif Cells Nanomed Biotechnol 2021; 49: 407-435.

[34] Zhang Q, Luan J, Song L, Wei X, Xia J and Song N. Malignant Evaluation and Clinical Prognostic Values of M6A RNA Methylation Regulators in Prostate Cancer. J Cancer 2021; 12: 3575-3586.

[35] Ji G, Huang C, He S, Gong Y, Song G, Li X and Zhou L. Comprehensive analysis of m6A regulators prognostic value in prostate cancer. Aging (Albany NY) 2020; 12: 14863-14884.

[36] Ou-Yang S, Liu JH and Wang QZ. Expression patterns and a prognostic model of m(6)A-associated regulators in prostate adenocarcinoma. Biomark Med 2020; 14: 1663-1677.

[37] Wang J, Lin H, Zhou M, Xiang Q, Deng Y, Luo L, Liu Y, Zhu Z and Zhao Z. The m6A methylation regulator-based signature for predicting the prognosis of prostate cancer. Future Oncol 2020; 16: 2421-2432.

[38] Wu Q, Xie X, Huang Y, Meng S, Li Y, Wang H and Hu Y. N6-methyladenosine RNA methylation regulators contribute to the progression of prostate cancer. J Cancer 2021; 12: 682-692.

[39] Liu B, Jiang HY, Yuan T, Luo J, Zhou WD, Jiang QQ and Wu D. Enzalutamide-Induced Upregulation of PCAT6 Promotes Prostate Cancer Neuroendocrine Differentiation by Regulating miR-326/HNRNPA2B1 Axis. Front Oncol 2021; 11: 650054.

[40] Jiang M, Lu Y, Duan D, Wang H, Man G, Kang C, Abulimiti K and Li Y. Systematic Investigation of mRNA N (6)-Methyladenosine Machinery in Primary Prostate Cancer. Dis Markers 2020; 2020: 8833438.

[41] Cheng Y, Li L, Qin Z, Li X and Qi F. Identification of castration-resistant prostate cancer-related hub genes using weighted gene co-expression network analysis. J Cell Mol Med 2020; 24: 8006-8017.

[42] Singh AN and Sharma N. Quantitative SWATH-Based Proteomic Profiling for Identification of Mechanism-Driven Diagnostic Biomarkers Conferring in the Progression of Metastatic Prostate Cancer. Front Oncol 2020; 10: 493.

[43] Peng Z, Andersson K, Lindholm J, Dethlefsen O, Pramana S, Pawitan Y, Nistér M, Nilsson S and Li C. Improving the Prediction of Prostate Cancer Overall Survival by Supplementing Readily Available Clinical Data with Gene Expression Levels of IGFBP3 and F3 in Formalin-Fixed Paraffin Embedded Core Needle Biopsy Material. PLoS One 2016; 11: e0145545.

[44] Prager AJ, Peng CR, Lita E, McNally D, Kaushal A, Sproull M, Compton K, Dahut WL, Figg WD, Citrin D and Camphausen KA. Urinary aHGF, IGFBP3 and OPN as diagnostic and prognostic biomarkers for prostate cancer. Biomarkers in medicine 2013; 7: 831-841.

[45] Qie Y, Nian X, Liu X, Hu H, Zhang C, Xie L, Han R, Wu C and Xu Y. Polymorphism in IGFBP3 gene is associated with prostate cancer risk: an updated meta-analysis. OncoTargets and therapy 2016; 9: 4163-4171.

[46] Zhang X, Wang D, Liu B, Jin X, Wang X, Pan J, Tu W and Shao Y. IMP3 accelerates the progression of prostate cancer through inhibiting PTEN expression in a SMURF1-dependent way. J Exp Clin Cancer Res 2020; 39: 190.

[47] Szarvas T, Tschirdewahn S, Niedworok C, Kramer G, Sevcenco S, Reis H, Shariat SF, Rübben H and vom Dorp F. Prognostic value of tissue and circulating levels of IMP3 in prostate cancer. Int J Cancer 2014; 135: 1596-1604.

[48] Ikenberg K, Fritzsche FR, Zuerrer-Haerdi U, Hofmann I, Hermanns T, Seifert H, Müntener M, Provenzano M, Sulser T, Behnke S, Gerhardt J, Mortezavi A, Wild P, Hofstädter F, Burger M, Moch H and Kristiansen G. Insulin-like growth factor II mRNA binding protein 3 (IMP3) is overexpressed in prostate cancer and correlates with higher Gleason scores. BMC Cancer 2010; 10: 341.

[49] Binnewies M, Roberts EW, Kersten K, Chan V, Fearon DF, Merad M, Coussens LM, Gabrilovich DI, Ostrand-Rosenberg S, Hedrick CC, Vonderheide RH, Pittet MJ, Jain RK, Zou W, Howcroft TK, Woodhouse EC, Weinberg RA and Krummel MF. Understanding the tumor immune microenvironment (TIME) for effective therapy. Nat Med 2018; 24: 541-550.

[50] Quail DF and Joyce JA. Microenvironmental regulation of tumor progression and metastasis. Nat Med 2013; 19: 1423-1437.

Figures

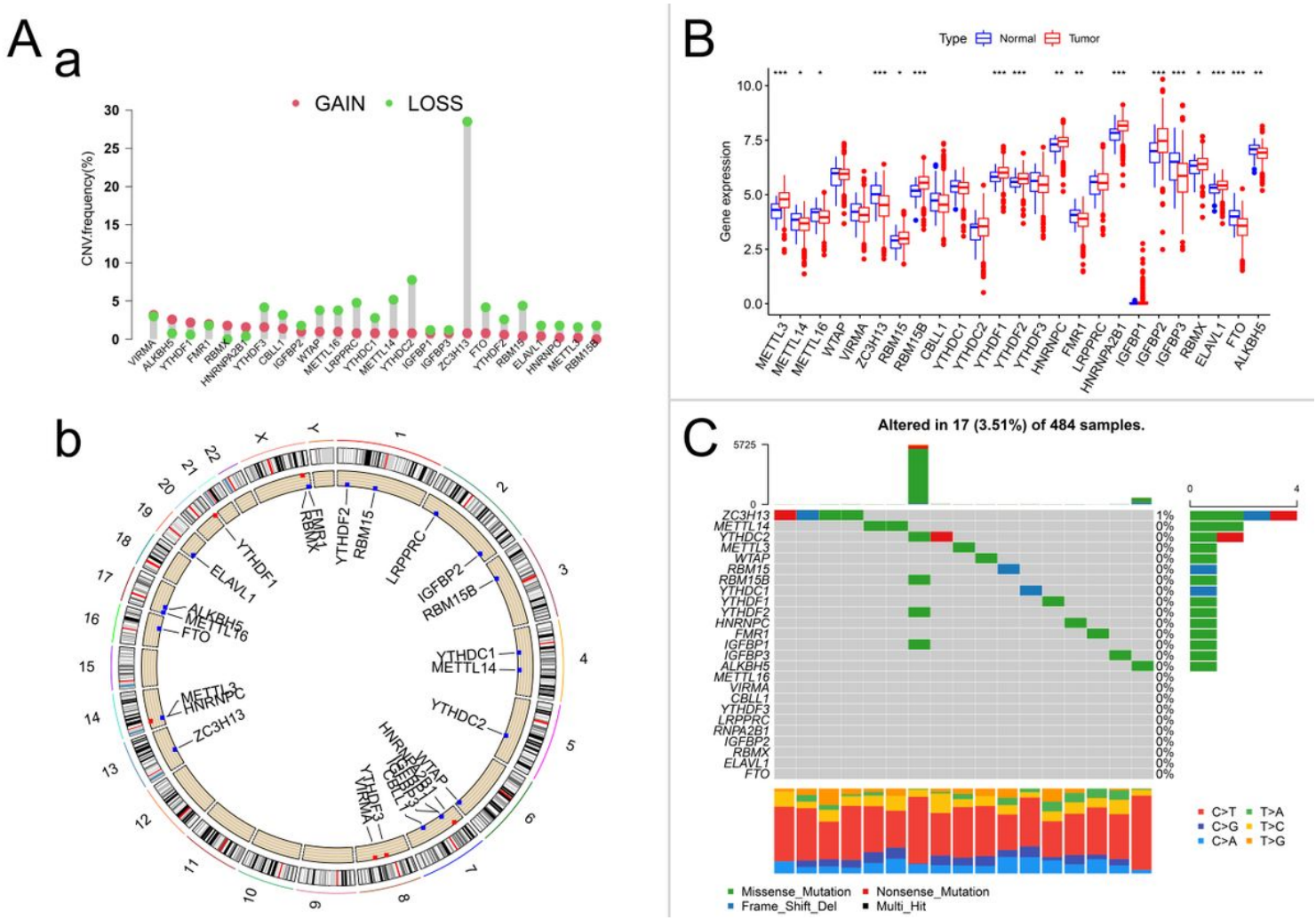

Figure 1

Characteristics of m6A regulators in prostate cancer. (A) (a) The CNV variation frequency of m6A regulators in TCGA-PRAD. Green dot: deletion frequency; red dot: amplification frequency. (b) The location of CNV alterations of m6A regulators on 23 chromosomes. (B) Box plot of expression of the 25 m6A regulators in PCa and normal tissues. Median values ± interquartile ranges are shown in the graph. * P < 0.05, ** P < 0.01, and *** P < 0.001. (C) The mutation frequency of 25 m6A regulators in 475 TCGA-PRAD patients is shown on the waterfall plot. The column represents individual patients, the upper bar plot shows the TMB, the right bar plot shows the proportion of each variant type, and the stacked bar plot below shows the transformed fraction of each patient.

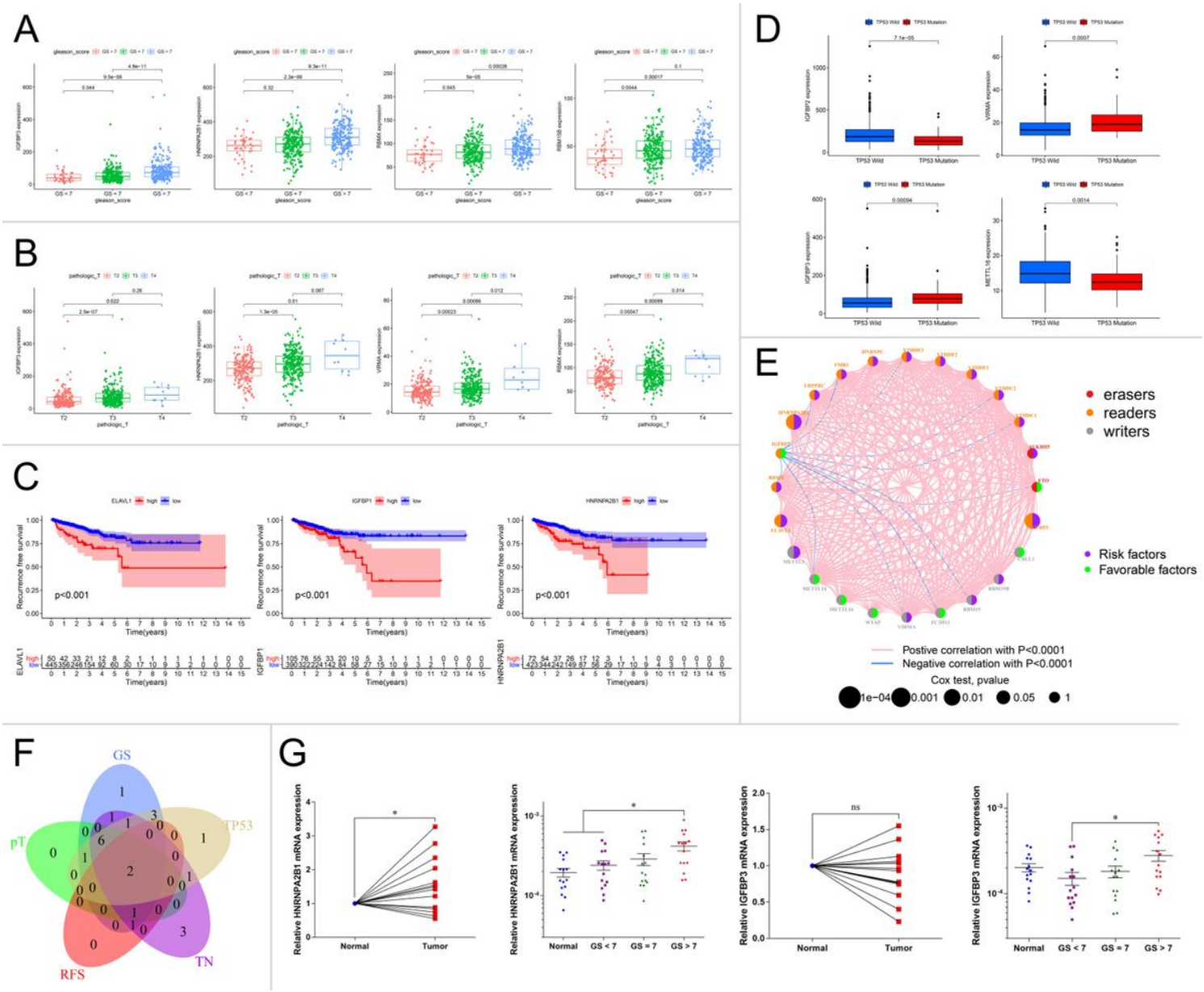

Figure 2

Expression of m6A regulators in relation to different PCa clinicopathological characteristics and prognoses. (A to D) Distribution of representative m6A regulators in TCGA-PRAD data stratified by GS (A), pT (B), RFS (C), and TP53 mutation (D). In the box plots, the median ± interquartile range of values is shown, and P values are given above each pair of comparisons. (E) Prognosis network of interactions between m6A regulators in PCa. The P values of each regulator on the prognosis are shown as circles of different sizes. Purple in the right hemisphere: risk factors for RFS; green in the right hemisphere: favorable factors for RFS. The erasers, readers, and writers of the m6A regulator are shown as red, orange, and gray colors, respectively, on the left. Positive or negative correlations of m6A regulators are linked with lines of different colors (pink: positive, blue: negative), and the correlation strength between them is shown as different line thicknesses. (F) Intersecting DEGs of 25 m6A regulators in GS (GS > 7 vs. GS < 7), pT (T3 vs. T2), RFS (P value of univariate Cox regression analysis < 0.05), TN (tumor vs. normal PCa tissues), and TP53 (mutation vs. wild type) are shown as Venn diagrams. (G) PCa tissues and

adjacent normal tissues were divided into four groups according to GS score (15 of normal tissue, 15 of GS ≤ 6, 15 of GS = 7, and 15 of GS ≥ 8). mRNA levels of intersecting genes were compared in different groups of PCa and adjacent normal tissues (PCa vs. adjacent normal; adjacent normal vs. GS ≤ 6 vs. GS = 7 vs. GS ≥ 8). Relative HNRNPA2B1 and IGFBP3 mRNA levels were assessed through qPCR analysis and normalized to adjacent normal tissues or those of endogenous reference genes. Means ± SEMs were shown in the graphs. * P < 0.05 and *** P < 0.001.

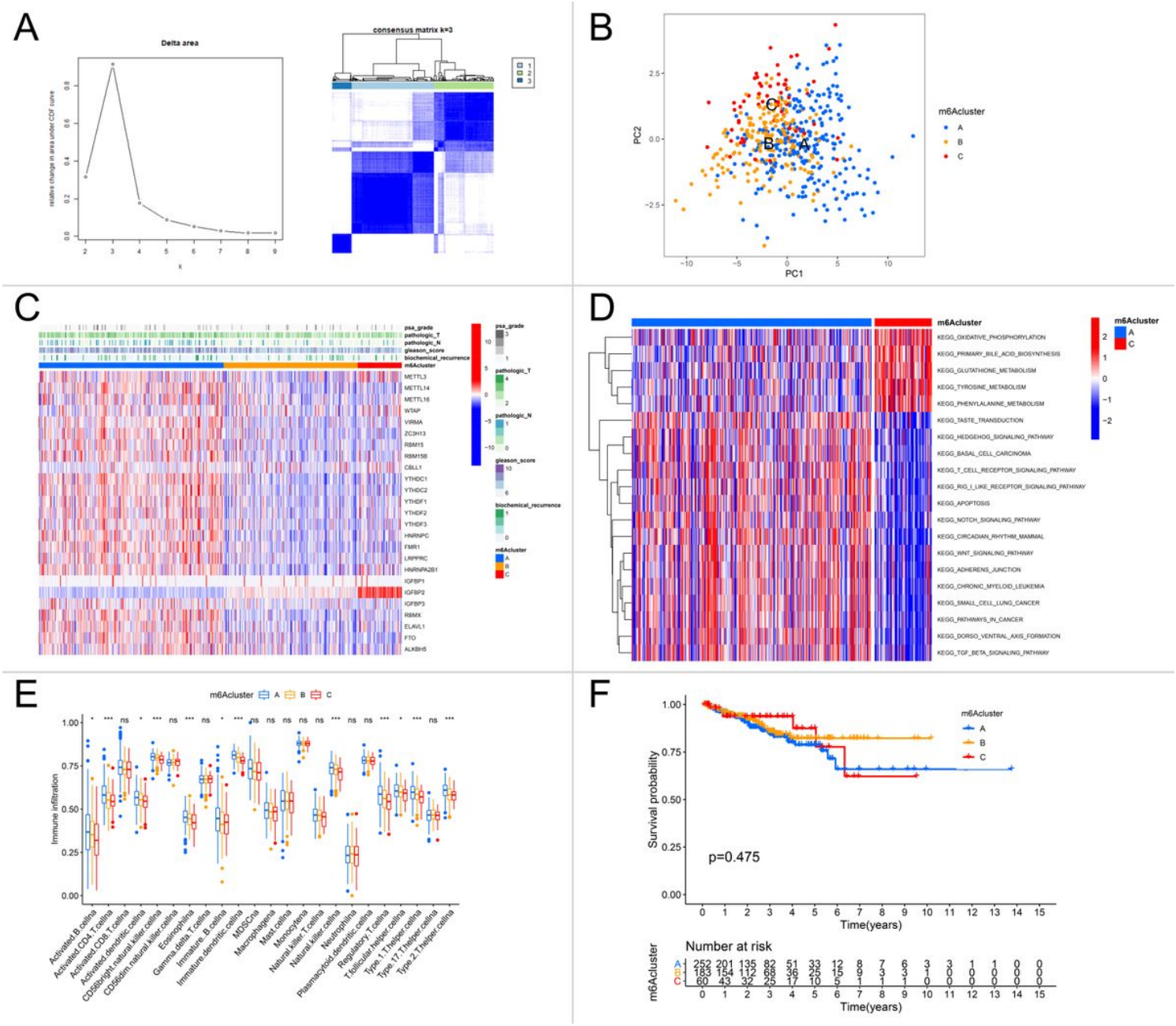

Figure 3

Consensus clustering analysis based on m6A regulators. (A) (left) Relative change in area under the CDF curve from k = 2 to 9. (right) Color-coded heatmap of the consensus matrix for k = 3. Color gradients represent values from 0–1 (white: 0, dark blue: 1). (B) PCA of the transcriptome profiles of three m6Acluster patterns, showing a marked difference in the transcriptome between different m6A clusters.

(C) The heatmap shows unsupervised clustering of 25 m6A regulators in TCGA-PRAD. PSA grade, pT, pN, GS, and biochemical recurrence were used for patient annotation. Red represents high expression, and blue represents low expression. (D) Heatmap of KEGG enrichment analysis showing the activation states of biological pathways in distinct m6Aclusters. Red represents activation, and blue represents inhibition. (E) Abundance of each infiltrating immune cell among the three m6Aclusters is shown in the boxplot. The median ± interquartile range of values is shown in the graph. ns P > 0.05; * P < 0.05; ***P < 0.001. (F) Survival analysis for RFS among three m6Aclusters based on 495 TCGA-PRAD patients. Kaplan-Meier curves and log-rank P values are shown in the graph, and the numbers at risk are shown at the bottom.

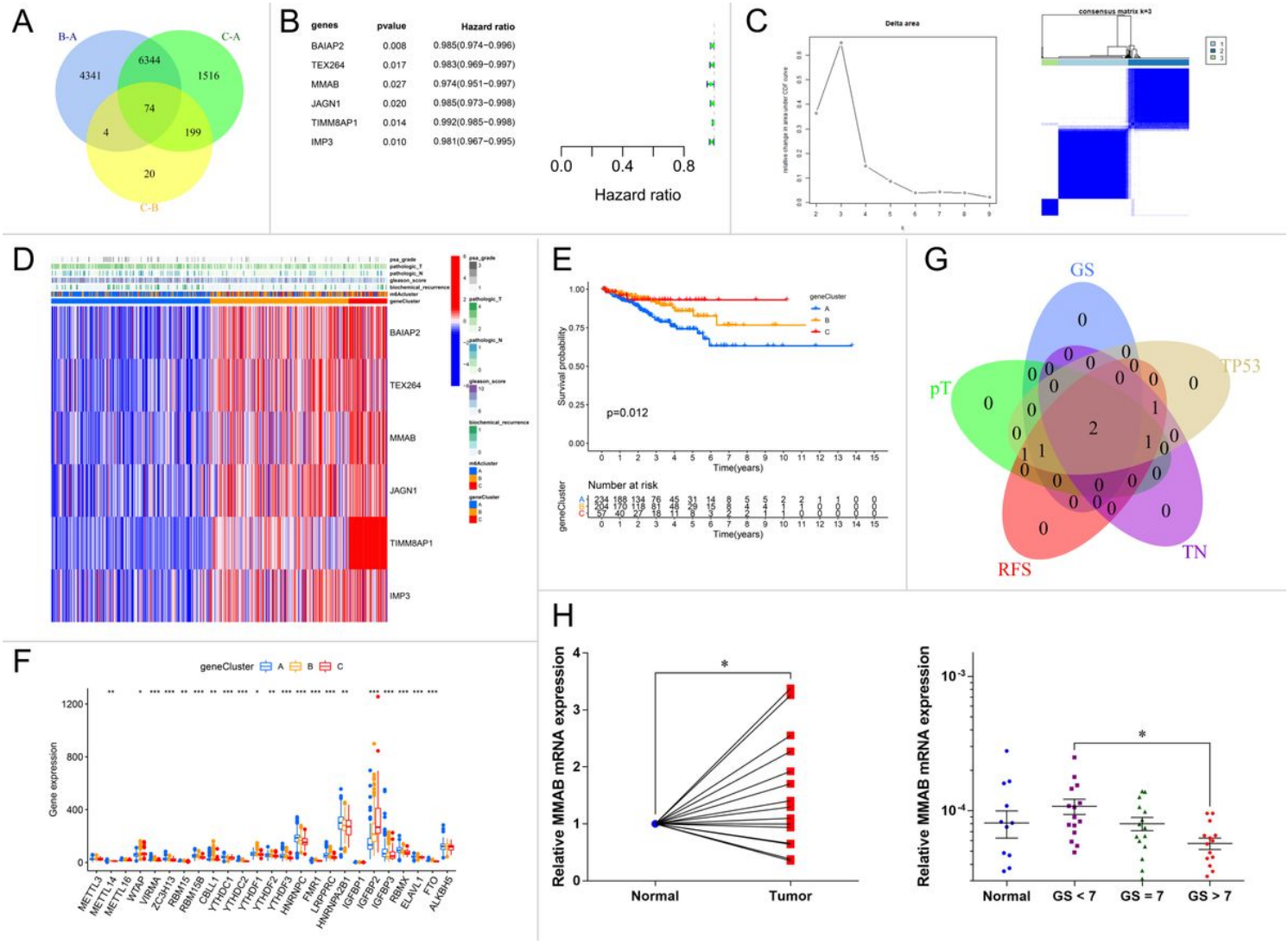

Figure 4

Consensus clustering analysis according to DEGs of m6A clusters. (A) DEGs were analyzed in every pairwise comparison of m6Aclusters and intersecting genes were identified via a Venn diagram. (B) Univariate Cox regression analysis was performed to evaluate RFS in relation to 74 intersecting genes. The statistical significance (P < 0.05) of 6 genes (BAIAP2, TEX264, MMAB, JAGN1, TIMM8AP1, and IMP3), P value, and HR value (with 95% CI) are shown in the plot. (C) Consensus clustering analysis according to DEGs of m6A clusters was performed. (left) Relative change in area under the CDF curve from k = 2 to 9. (right) Color-coded heatmap of the consensus matrix for k = 3. Color gradients represent

values from 0–1 (white: 0, dark blue: 1). (D) The heatmap shows unsupervised clustering of the 6 genes in TCGA-PRAD. PSA grade, pT, pN, GS, and biochemical recurrence were used for patient annotation. (E) Survival analysis for RFS among three geneClusters based on 495 TCGA-PRAD patients. Kaplan-Meier curves and log-rank P values are shown in the graph, and the numbers at risk are shown at the bottom. (F) Expression of m6A regulators among three geneClusters is shown in the boxplot. The median ± interquartile range of values is shown in the graph. ns P > 0.05; * P < 0.05; ** P < 0.01; ***P < 0.001. (G) As described in Fig. 2F, intersecting DEGs of GS, pT, RFS, TN, and TP53 are shown in a Venn diagram. (H) As described in Fig. 2G, PCa tissues and adjacent normal tissues were divided into four groups, and mRNA levels of intersecting genes (MMAB) were compared. * P < 0.05 and ** P < 0.01.

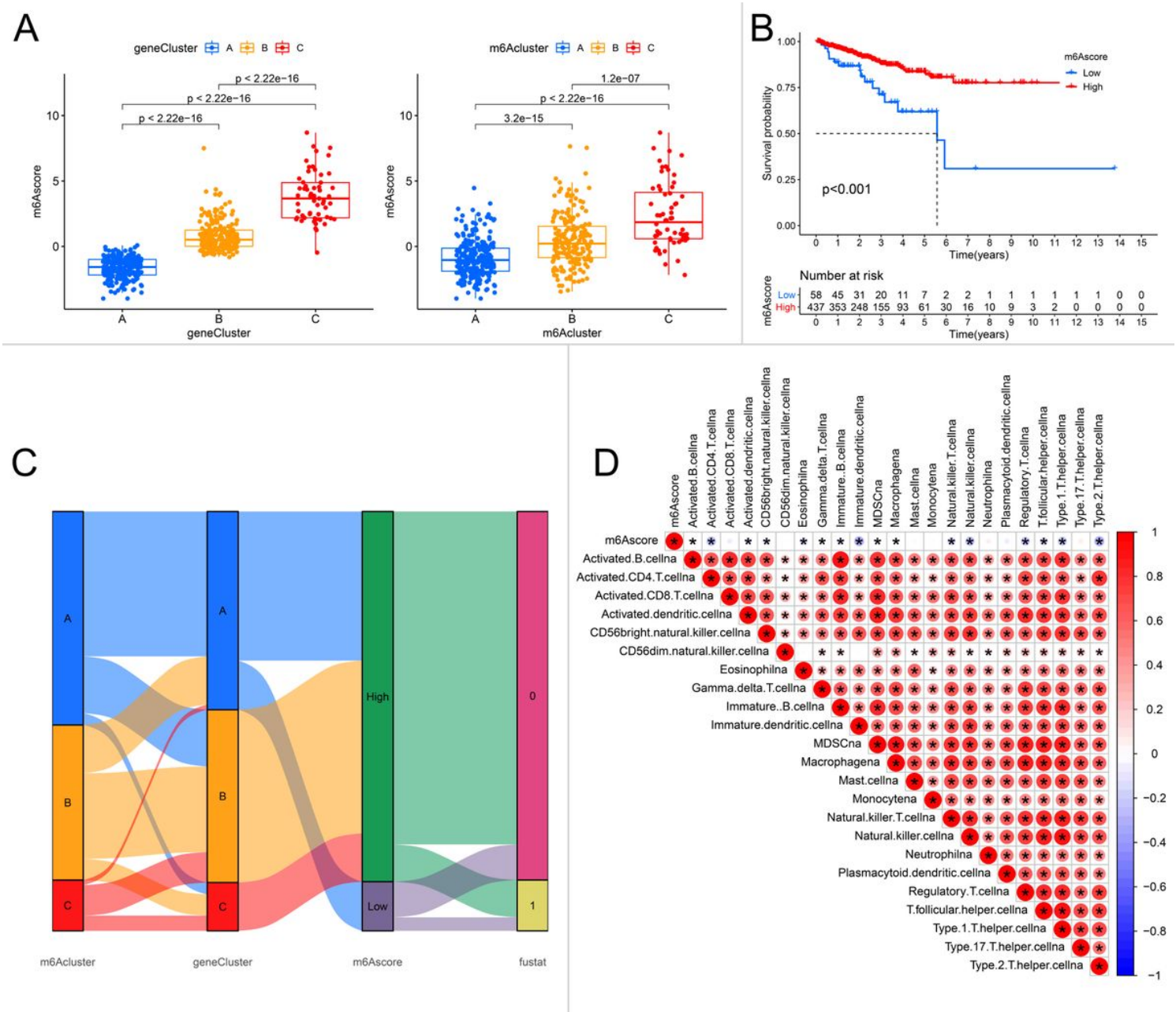

Figure 5

The low m6Ascore group based on the 6 genes was associated with poor prognosis in RFS. (A) The m6Ascore was calculated through PCA of the 6 gene levels in TCGA-PARD, and m6Ascores among geneClusters (left) and m6Aclusters (right) were compared. The median ± interquartile range of values and P values of the Kruskal-Wallis test are shown in the box plots. (B) PRAD patients were divided into low and high m6Ascore groups based on the optimum threshold segmentation of m6Ascores in relation to RFS. The prognosis of the two groups was evaluated through survival analysis. (C) Alluvial diagram showing changes in m6A clusters, geneClusters, m6Ascore, and recurrence status (fustat of 0: no biochemical recurrence, 1: biochemical recurrence). (D) Correlations between m6Ascore and immune cell infiltration in TCGA-PRAD using Spearman analysis. Red: positive correlation, blue: negative correlation.

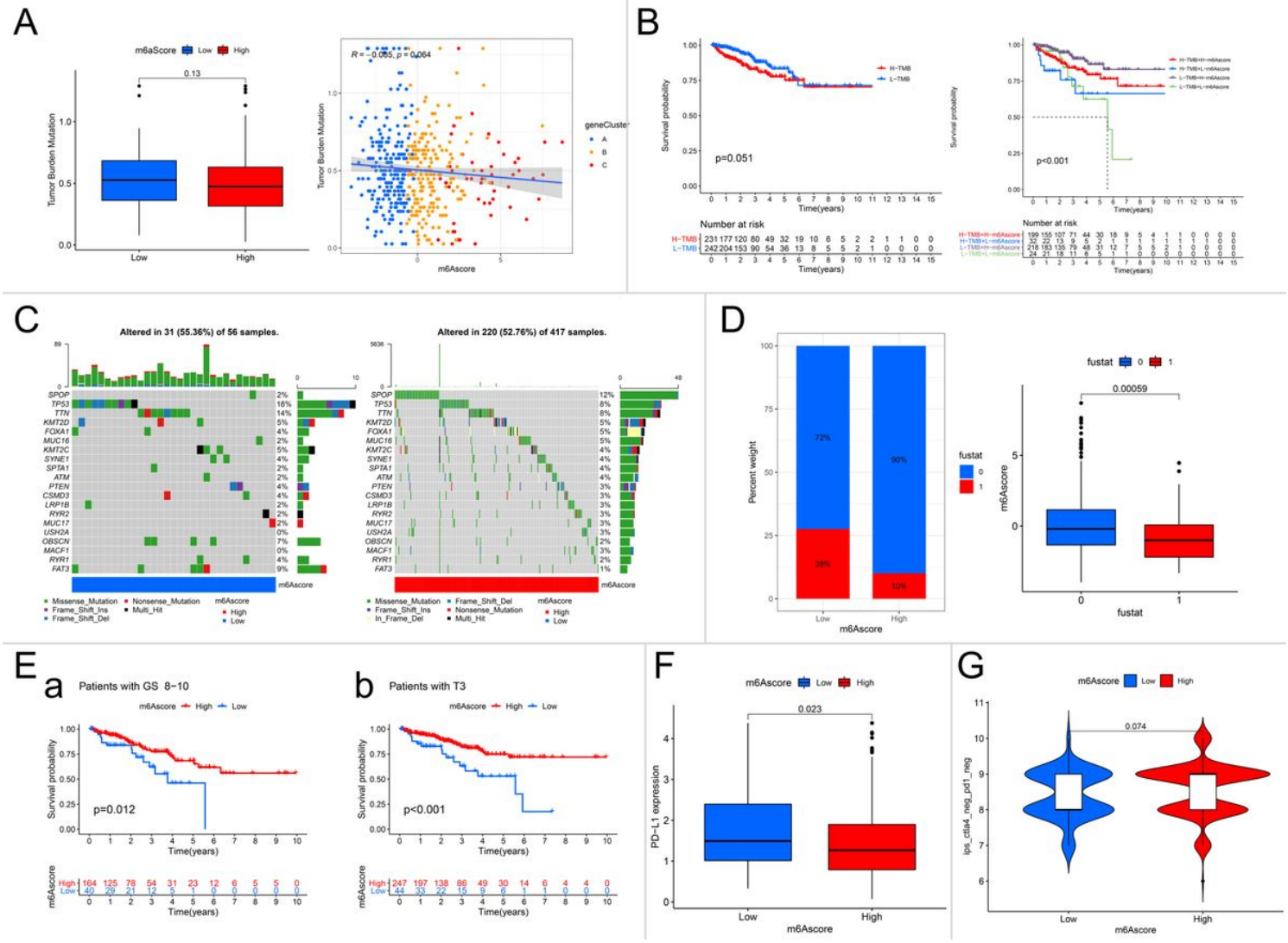

Figure 6

Characteristics of m6Ascore status in TCGA-PRAD tumor mutation and subtypes. (A) (left) TMB values in low and high m6Ascore groups. The P value of the Wilcoxon test is shown in box plots. (right) Correlation analysis of m6Ascore and TMB value in PCa was performed through Spearman correlation analysis. Different points of blue, orange, and red points in the scatter diagram represent geneClusters A to C, respectively. (B) (left) PRAD patients were divided into low and high TMB groups based on the optimum

threshold segmentation of TMB values in relation to RFS. Survival analysis of the two groups is shown in the graph. (right) PRAD patients were divided into four groups based on TMB and m6Ascore status (high (H)-TMB + H-m6Ascore; H-TMB + low (L)-m6Ascore; L-TMB + H-m6Ascore; and L-TMB + L-m6Ascore), and survival analysis was performed. (C) The waterfall plot of tumor somatic mutations in PRAD with low m6Ascore (left) and high m6Ascore (right). (D) (left) The proportion of biochemical recurrence status in m6Ascore groups (fustat of 0: no recurrence, 1: recurrence). (right) m6Ascore in different biochemical recurrence statuses. The P value of the Wilcoxon test is shown in box plots. (E) Survival analysis of different m6Ascore groups among TRAD patients with GS 8–10 (left) and pT3 (right). (F) Box plot of PD-L1 expression in low and high m6Ascore groups. The P value of the Wilcoxon test is shown in box plots. (G) Violin plot of IPS scores (CTLA4 negative and PD1 negative) in respective m6Ascore groups. The P value of the Wilcoxon test is shown in box plots.

Supplementary Files

This is a list of supplementary files associated with this preprint. Click to download.

- SupplementalFigures.docx
- supplementarytable.docx